Exchange of electric and magnetic resonances in multilayered metal/dielectric nanoplates

De Li,[1,2] Ling Qin,[1] Xiang Xiong,[1] Ru-Wen Peng,[1,*] Qing Hu,[1] Guo-Bin Ma,[1] Hao-Shen Zhou,[2] and Mu Wang[1]

[1]*National Laboratory of Solid State Microstructures and Department of Physics, Nanjing University, Nanjing 210093, China*

[2]*Energy Technology Research Institute, National Institute of Advanced Industrial Science and Technology, Umezono 1-1-1, Tsukuba, 305-8568, Japan*

*rwpeng@nju.edu.cn

Abstract: In this work, we have experimentally demonstrated that in a rectangular multilayered Ag/SiO_2 nanoplate array, electric and magnetic resonances are exchanged at the same frequency simply by changing the polarization of incident light for 90°. Both electric and magnetic resonances originate from localized surface plasmons, and lead to negative permittivity and permeability, respectively. The numerical calculations on electromagnetic fields agree with the experiments. The investigations provide a simple building block for a metamaterial to switch electric and magnetic resonances by external excitation field.

OCIS codes: (160.3918) Metamaterials; (250.5403) Plasmonics; (260.5740) Resonance; (350.3618) Left-handed materials.

References and links

1. J. B. Pendry, A. J. Holden, D. J. Robbins, and W. J. Stewart, "Magnetism from Conductors and Enhanced Nonlinear Phenomena," IEEE Trans. Microw. Theory Tech. **47**(11), 2075–2084 (1999).
2. D. R. Smith, W. J. Padilla, D. C. Vier, S. C. Nemat-Nasser, and S. Schultz, "Composite medium with simultaneously negative permeability and permittivity," Phys. Rev. Lett. **84**(18), 4184–4187 (2000).
3. T. W. Ebbesen, H. J. Lezec, H. F. Ghaemi, T. Thio, and P. A. Wolff, "Extraordinary optical transmission through sub-wavelength hole arrays," Nature **391**(6668), 667–669 (1998).
4. A. Battula, S. Chen, Y. Lu, R. J. Knize, and K. Reinhardt, "Tuning the extraordinary optical transmission through subwavelength hole array by applying a magnetic field," Opt. Lett. **32**(18), 2692–2694 (2007).
5. Y. J. Bao, R. W. Peng, D. J. Shu, M. Wang, X. Lu, J. Shao, W. Lu, and N. B. Ming, "Role of interference between localized and propagating surface waves on the extraordinary optical transmission through a subwavelength-aperture array," Phys. Rev. Lett. **101**(8), 087401 (2008).
6. Z. J. Zhang, R. W. Peng, Z. Wang, F. Gao, X. R. Huang, W. H. Sun, Q. J. Wang, and M. Wang, "Plasmonic antenna array at optical frequency made by nanoapertures," Appl. Phys. Lett. **93**(17), 171110 (2008).
7. J. B. Pendry, "Negative refraction makes a perfect lens," Phys. Rev. Lett. **85**(18), 3966–3969 (2000).
8. X. Zhang and Z. W. Liu, "Superlenses to overcome the diffraction limit," Nat. Mater. **7**(6), 435–441 (2008).
9. J. B. Pendry, D. Schurig, and D. R. Smith, "Controlling electromagnetic fields," Science **312**(5781), 1780–1782 (2006).
10. T. J. Yen, W. J. Padilla, N. Fang, D. C. Vier, D. R. Smith, J. B. Pendry, D. N. Basov, and X. Zhang, "Terahertz magnetic response from artificial materials," Science **303**(5663), 1494–1496 (2004).
11. S. Linden, C. Enkrich, M. Wegener, J. F. Zhou, T. Koschny, and C. M. Soukoulis, "Magnetic response of metamaterials at 100 terahertz," Science **306**(5700), 1351–1353 (2004).
12. G. Dolling, C. Enkrich, M. Wegener, J. F. Zhou, C. M. Soukoulis, and S. Linden, "Cut-wire pairs and plate pairs as magnetic atoms for optical metamaterials," Opt. Lett. **30**(23), 3198–3200 (2005).
13. T. Pakizeh, M. S. Abrishamian, N. Granpayeh, A. Dmitriev, and M. Käll, "Magnetic-field enhancement in gold nanosandwiches," Opt. Express **14**(18), 8240–8246 (2006).
14. S. Zhang, W. J. Fan, N. C. Panoiu, K. J. Malloy, R. M. Osgood, and S. R. J. Brueck, "Experimental demonstration of near-infrared negative-index metamaterials," Phys. Rev. Lett. **95**(13), 137404 (2005).
15. K. H. Su, Q. H. Wei, and X. Zhang, "Tunable and augmented plasmon resonances of Au/SiO_2 /Au nanodisks," Appl. Phys. Lett. **88**(6), 063118 (2006).
16. X. Z. Wei, H. F. Shi, X. C. Dong, Y. G. Lu, and C. L. Du, "A high refractive index metamaterial at visible frequencies formed by stacked cut-wire plasmonic structures," Appl. Phys. Lett. **97**(1), 011904 (2010).
17. Z. H. Tang, R. W. Peng, Z. Wang, X. Wu, Y. J. Bao, Q. J. Wang, Z. J. Zhang, W. H. Sun, and M. Wang, "Coupling of surface plasmons in nanostructured metal/dielectric multilayers with subwavelength hole arrays," Phys. Rev. B **76**(19), 195405 (2007).

#154745 - $15.00 USD Received 16 Sep 2011; revised 16 Oct 2011; accepted 16 Oct 2011; published 27 Oct 2011

18. X. Xiong, W. H. Sun, Y. J. Bao, R. W. Peng, M. Wang, C. Sun, X. Lu, J. Shao, Z. F. Li, and N. B. Ming, "Switching the electric and magnetic responses in a metamaterial," Phys. Rev. B **80**(20), 201105 (2009).
19. X. Xiong, X.-C. Chen, M. Wang, R.-W. Peng, D.-J. Shu, and C. Sun, "Optically nonactive assorted helix array with interchangeable magnetic/electric resonance," Appl. Phys. Lett. **98**(7), 071901 (2011).
20. D. Li, L. Qin, D. X. Qi, F. Gao, R. W. Peng, J. Zou, Q. J. Wang, and M. Wang, "Tunable electric and magnetic resonances in multilayered metal/dielectric nanoplates at optical frequencies," J. Phys. D Appl. Phys. **43**(34), 345102 (2010).
21. A. D. Rakic, A. B. Djurisic, J. M. Elazar, and M. L. Majewski, "Optical properties of metallic films for vertical-cavity optoelectronic devices," Appl. Opt. **37**(22), 5271–5283 (1998).
22. V. M. Shalaev, W. Cai, U. K. Chettiar, H. K. Yuan, A. K. Sarychev, V. P. Drachev, and A. V. Kildishev, "Negative index of refraction in optical metamaterials," Opt. Lett. **30**(24), 3356–3358 (2005).
23. D. R. Smith, S. Schultz, P. Markoš, and C. M. Soukoulis, "Determination of effective permittivity and permeability of metamaterials from reflection and transmission coefficients," Phys. Rev. B **65**(19), 195104 (2002).
24. T. Koschny, P. Markoš, D. R. Smith, and C. M. Soukoulis, "Resonant and antiresonant frequency dependence of the effective parameters of metamaterials," Phys. Rev. E Stat. Nonlin. Soft Matter Phys. **68**(6), 065602 (2003).
25. M. Meier, A. Wokaun, and P. F. Liao, "Enhanced fields on rough surfaces: dipolar interactions among particles of sizes exceeding the Rayleigh limit," J. Opt. Soc. Am. B **2**(6), 931–949 (1985).

In the past decade, metamaterials have drivingly developed, which provides a new paradigm to control the electromagnetic properties of materials beyond the nature. With deliberately designed metallic microstructures, specific electromagnetic responses are realized, such as artificial magnetism [1, 2], extraordinary optical transmission [3–5], optical antenna [6], subwavelength imaging [7, 8] and invisible cloaking [9]. As we know, there are no high-frequency magnetic materials in nature. However, the high-frequency magnetic response of a metamaterial can be achieved by the interaction of magnetic component of incident light and induced magnetic dipole moment. Recently, some engineered metallic structures have been investigated, in which magnetic resonances can be excited from microwave to optical frequencies, such as double split-ring resonators (SRRs) [1, 10], coupled metal nano-strips [11], the metal wire pairs [12], gold nanosandwiches [13], fishnet structures [14] and so on. At optical frequencies, the metal-dielectric-metal nanosandwich is very common as a resonant magnetic structure, however, few efforts have been made to exploit multilayerd metal/dielectric nanostructures [15, 16], where the coupling of surface plasmons may play an important role [17].

The electric and magnetic responses of a system are usually characterized by permittivity and permeability. It has been reported that the electric and magnetic responses strongly depend on the external excitation field [18, 19], which achieve a unique way to tailor permittivity and permeability of the structure. In our previous work [20], the electromagnetic responses in multilayered Ag/SiO_2 nanoplates at optical frequencies have been investigated, where electric and magnetic resonances can be tailored by the geometrical parameters of the nanoplates. Based on this knowledge, in present work, we try to change the geometry of the nanoplate to tune the electric and magnetic resonances at same frequency. We have experimentally demonstrated that in a rectangular multilayered Ag/SiO_2 nanoplate array, electric and magnetic resonances are exchanged at the same frequency simply by changing the polarization of incident light for 90°. Both electric and magnetic resonances originate from localized surface plasmons (LSPs), and lead to negative permittivity and permeability, respectively. The investigations may provide another way to achieve optical magnetism by switching electric resonance to magnetic one, which may be used to construct specific negative-index materials.

#154745 - $15.00 USD Received 16 Sep 2011; revised 16 Oct 2011; accepted 16 Oct 2011; published 27 Oct 2011

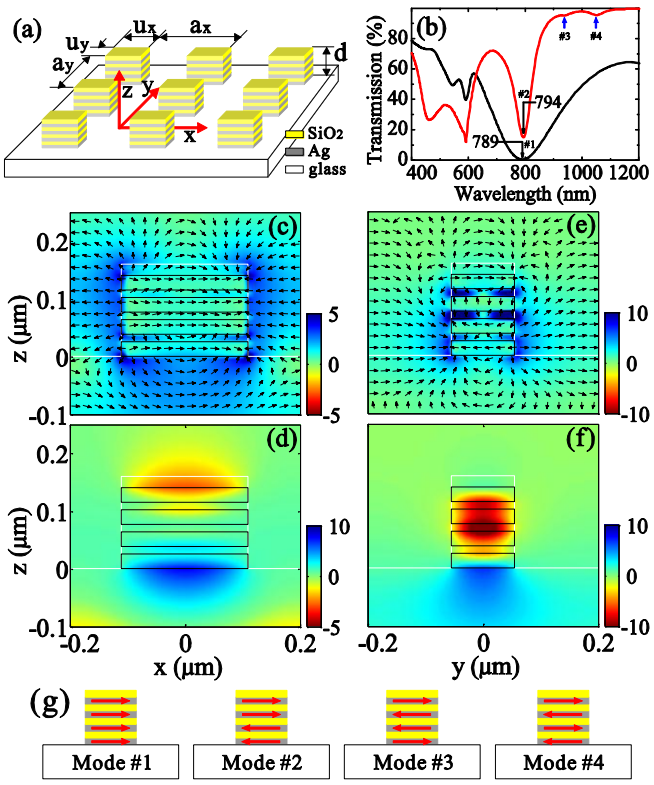

Fig. 1. (a) Schematic view of multilayered Ag/SiO_2 nanoplates on a glass substrate with periodicities of the square lattice $a_x = a_y = 400\,\text{nm}$, and widths of the rectangular nanoplate $u_x = 220\,\text{nm}$ and $u_y = 110\,\text{nm}$. The layer sequence from the glass substrate to the top is $Ag/SiO_2/Ag/SiO_2/Ag/SiO_2/Ag/SiO_2$ with a total thickness $d = 160\,\text{nm}$, where all Ag layers are 25 nm thick and SiO_2 layers are 13.3 nm thick except the topmost SiO_2 layer of 20 nm thick. (b) The calculated normal transmission spectra for the structure described in (a), which is illuminated from the glass substrate by the x-polarized (black curve) and y-polarized (red curve) incident light, respectively. The x-z plane cross section of (c) the electric field distribution E where the arrows represent direction and the color map represents intensity and (d) the magnetic field distribution H_y for the electric resonance (Mode #1) in the x-polarized incidence. The y-z plane cross section of (e) the electric field distribution E and (f) the magnetic field distribution H_x for the magnetic resonance (Mode #2) in the y-polarized incidence. Here, the black boxes and the white line represent Ag layers and the boundary of air, respectively. (g) Schematics of the effective currents induced in multiple Ag layers for the four optical modes marked in (b), respectively.

Firstly, we have designed a rectangular multilayered Ag/SiO_2 nanoplate array (as shown in Fig. 1(a)). Optical properties of this nanoplate array are calculated based on the full-vectorial three-dimensional finite-difference time-domain (FDTD) method. In the simulations, the frequency-dependent permittivity of Ag is obtained from the Lorentz-Drude model [21]. Figure 1(b) shows the normal transmission spectra when the light along z axis illuminates this structure from the glass substrate. In the x-polarized incidence (black curve), there is a broad transmission dip (marked as Mode #1) at the wavelength $\lambda = 789\,\text{nm}$, while there is a narrow dip (marked as Mode #2) at $\lambda = 794\,\text{nm}$ in the y-polarized incidence (red curve). Although two dips are located at the same wavelength $\lambda \cong 800\,\text{nm}$, they originate from the electric and magnetic resonances, respectively. Figures 1(c) and (d) illustrate the electric field distribution E and the magnetic field distribution H_y in the x-z plane for the electric resonance (Mode #1). The electric fields in all Ag layers are in the same directions, and the electric field around

#154745 - $15.00 USD Received 16 Sep 2011; revised 16 Oct 2011; accepted 16 Oct 2011; published 27 Oct 2011

the nanoplate is very strong, especially at four corners. The magnetic field H_y in the center of the nanoplate is weak while those on top and bottom of the nanoplate are quite strong with opposite directions. Obviously, the LSPs on multiple Ag layers are in-phase coupled, which lead to the electric resonance. In contrast, the magnetic resonance results from the out-of-phase coupling of LSPs on multiple Ag layers [20]. For Mode #2, as shown in Figs. 1(e) and (f), the electric fields in the upper and lower Ag layers are in the opposite directions, and the electric fields are very strong with opposite directions between left and right sides in SiO_2 layers; while the magnetic fields are strong within the multiayer structure. All these phenomena indicate that the Mode #2 comes from the magnetic resonance.

It is interestingly noted that there are more than two optical modes excited in the structure (as shown in Fig. 1(b)). Due to the fact that the diffraction is strong enough and optical excitation becomes complicated when the wavelength is less than 600nm or so, we simply pay attention to the cases when the wavelength is larger than 600nm. As marked in Fig. 1(b), four transmission dips appear in both x-polarized and y-polarized incidences when $\lambda > 600\,\mathrm{nm}$. By calculating the electromagnetic filed distributions at these dips, the local currents in the layer structure can be obtained, which are effectively illustrated by the highlighted arrows in Fig. 1(g). For Mode #1, the effective currents in four Ag layers are in parallel and form the effective electric dipoles, which is the symmetric excitation corresponding to the electric resonance (as discussed above); while for Mode #2, the effective currents in the upper two Ag layers are in parallel, and the currents in lower two Ag layers are in anti-parallel with those in upper two layers. Therefore, the effective circular currents are induced and form the effective magnetic dipole, that is, Mode #2 is antisymmetric excitation corresponding to the magnetic resonance (as discussed above). Mode #1 and Mode #2 are similar to the excitations in two-Ag-layer-coupled systems [22]. As for Mode #3 and Mode #4, both of them are antisymmetric excitations. The magnetic fields induced by circular currents in Mode #3 and Mode #4 may cancel each other, thereafter, these two excitations becomes weak.

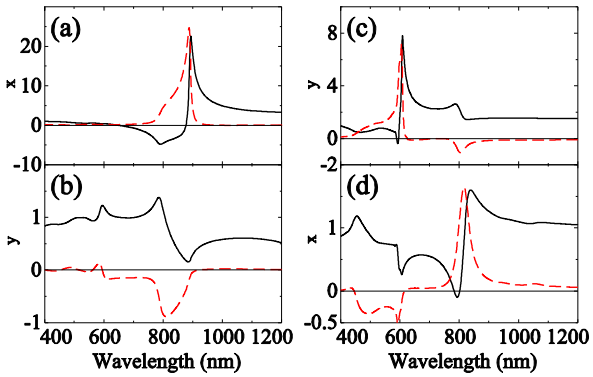

Fig. 2. (a) The retrieved permittivity ε_x and (b) permeability μ_y for the nanoplates illuminated by the x-polarized normal incidence, while (c) ε_y and (d) μ_x for the y-polarized incidence. Here, the black solid and red dashed curves stand for the real and imaginary parts, respectively.

Now we try to give more evidence to illustrate the electric resonance (Mode #1) and the magnetic resonance (Mode #2) at $\lambda \cong 800\,\mathrm{nm}$. We consider the whole structure effectively as a homogeneous slab with the thickness $d = 160\,\mathrm{nm}$ between the glass substrate and the air, and derive the effective permittivity ε and permeability μ from normal reflection and transmission coefficients, analysed by a robust retrieval algorithm [23]. In the x-polarized incidence, there is a relatively wide negative electric response around the wavelength $\lambda \cong 800\,\mathrm{nm}$, as shown in Fig. 2(a). Meanwhile, the electric resonance introduces a magnetic anti-resonance response [24], as an evident drop of $\mathrm{Re}(\mu_y)$ and a negative value of

#154745 - $15.00 USD Received 16 Sep 2011; revised 16 Oct 2011; accepted 16 Oct 2011; published 27 Oct 2011

$\mathrm{Im}(\mu_y)$ in Fig. 2(b). Actually, the magnetic anti-resonance always accompanies with the electric resonance, because the anti-resonance is intrinsic in a metamaterial owing to the finite spatial periodicity. During the resonance, the magnetic field is gained with negative $\mathrm{Im}(\mu_y)$, but the electric filed is attenuated with positive $\mathrm{Im}(\varepsilon_x)$, as shown in Fig. 2(a). Thereafter, the total energy is not gained and the system still obeys the conversation of energy. While in the y-polarized incidence, the magnetic resonance results in a narrow band of negative magnetic response and introduces a weak electric anti-resonance response at the wavelength $\lambda \cong 800\,\mathrm{nm}$, as shown in Fig. 2(d) and (c) respectively. (Here, the electric anti-resonance can be analog to the above magnetic anti-resonance.) These properties confirm the electric and magnetic resonances, which can be switched at the same frequency by changing the polarization of incident light for 90°.

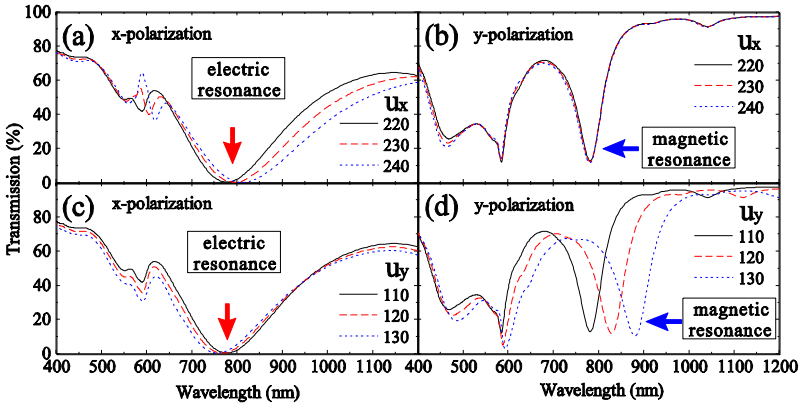

Fig. 3. The calculated normal transmission spectra of rectangular nanoplates with varying the long width u_x for (a) x-polarization and (b) y-polarization, and varying the short width u_y for (c) x-polarization and (d) y-polarization. Here, $u_x = 220, 230 \text{ and } 240\,\mathrm{nm}$ and $u_y = 110\,\mathrm{nm}$ for (a) and (b), and $u_y = 110, 120 \text{ and } 130\,\mathrm{nm}$ and $u_x = 220\,\mathrm{nm}$ for (c) and (d).

It should be mentioned that only by optimizing the widths of the nanoplates, the electric and magnetic resonances coincide at the same wavelength $\lambda \cong 800\,\mathrm{nm}$ in different polarization excitations. The electric and magnetic resonances are tuned by changing the widths of the nanoplates (as shown in Fig. 3). When the short width is fixed as $u_y = 110\,\mathrm{nm}$ but the long width is varied as $u_x = 220, 230 \text{ and } 240\,\mathrm{nm}$, the electric resonance shifts a little to the red for the x-polarization as shown in Fig. 3(a), and the magnetic resonance does not move for the y-polarization as shown in Fig. 3(b). In contrast, when the long width is fixed as $u_x = 220\,\mathrm{nm}$ and the short width is tuned as $u_y = 110, 120 \text{ and } 130\,\mathrm{nm}$, the electric resonance shifts a little to the blue for the x-polarization as shown in Fig. 3(c), while the magnetic resonance dramatically shift to the red for the y-polarization as shown in Fig. 3(d). Therefore, the electric resonance depends on both widths of the nanoplates differently, while the magnetic resonance only determined by the width along polarization, as discussed in Ref. 20.

In experiments, a nanoplate array was fabricated by using magnetron sputtering and focused-ion-beam (FIB) facility, and its optical spectra were measured by a micro-spectrophotometer. First, a multilayered Ag/SiO_2 film was coated on a piece of glass substrate by magnetron sputtering, then an array of nanoplates was fabricated on the film by focused-ion-beam facility (strata FIB 201, FEI company, 30 keV Ga ions). Figures 4(a) and (b) shows the field-emission scanning electronic microscope (SEM) images of the sample, where the bars represent $1\,\mu\mathrm{m}$ and 200 nm, respectively. And the layer sequence is revealed by the SEM images of side view with a 30° tilt-angle, as shown in Figs. 4(c) and (d) where both the

#154745 - $15.00 USD Received 16 Sep 2011; revised 16 Oct 2011; accepted 16 Oct 2011; published 27 Oct 2011

bars represent 100 nm. The average parameters of this sample are close to the theoretical design. However, the nanoplates are a little nonuniform in the array with the sidewall angle of about 15°, and some of the glass substrate is sculpted by the ion beam.

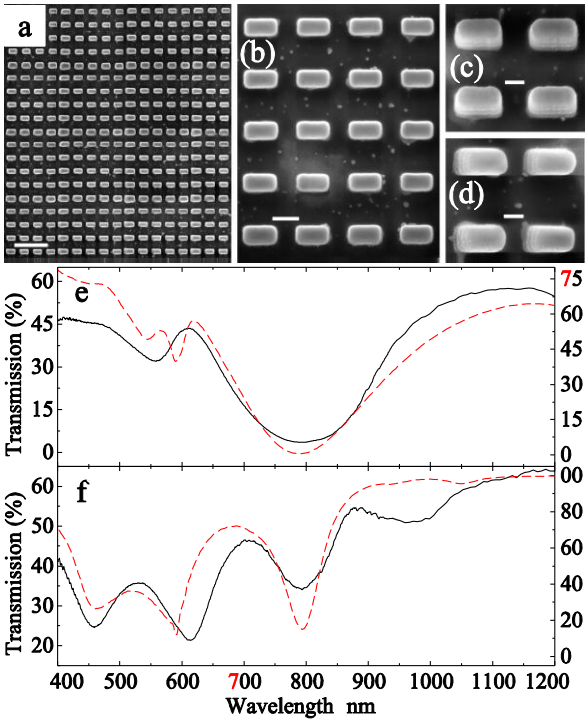

Fig. 4. (a) and (b) The SEM images of multilayered Ag/SiO_2 nanoplates on a glass substrate, where the bars represent 1 μm and 200 nm, respectively. (c) and (d) The SEM images of side view with a 30° tilt-angle, where both the bars represent 100 nm. Here, the parameters of this sample are nearly the same as that model. (e) and (f) the measured normal transmission spectra for the incident polarization parallel and perpendicular to the long width, respectively, where the red dashed curves are calculated spectra in Fig. 1(b).

Using a UV-visible-NIR microspectrophotometer (CRAIC QDI2010), we measured the normal transmission spectra of the sample. For the incident polarization parallel to the long width, there are two dips at $\lambda \cong 550$ and 800 nm, as the black solid curve in Fig. 4(e). For the other polarization, there are four transmission dips at $\lambda \cong 450, 600, 800$ and 950 nm, as shown in Fig. 4(f). Obviously, the measured spectra agree with the calculated (Figs. 4(e) and (f), red dashed) excellently, except for the dull dip at $\lambda \cong 950$ nm. As we discussed before, the dips at $\lambda \cong 800$ nm arise from the electric and magnetic resonances, respectively. Additionally, the dips at $\lambda \cong 450$ and 550 nm are related to propagating surface plasmons [5], the dip at $\lambda \cong 600$ nm takes place when a new diffracted beam emerges [25].

In order to understand the measured data better, we also carried out the calculations for the nanoplates with oblique side walls (schematically shown in Fig. 5(a)). For example, in a tapered nanoplate, the top widths of the rectangular nanoplate are set as $u_x = 199$ nm and $u_y = 89$ nm, and the bottom widths are set as $u_x = 241$ nm and $u_y = 131$ nm, respectively. The tilt angle of the side wall is about 15°. Except for the widths, the other parameters are kept the same as the straight nanoplate array. Figure 5(b) shows the calculated transmission of the tapered nanoplate array for both polarizations, where all the dips are changed a little owing to the variation of widths. Corresponding to four typical modes marked in Fig. 5(b), the effective currents induced in multiple Ag layers are illustrated in Fig. 5(c), respectively. We find that

#154745 - $15.00 USD Received 16 Sep 2011; revised 16 Oct 2011; accepted 16 Oct 2011; published 27 Oct 2011

both the electric resonance (Mode #1) and the magnetic resonance (Mode #2) depend on the average width in the tapered nanoplate. The dips of electric and magnetic resonances keep at $\lambda \cong 800\,\text{nm}$, as the average widths in each direction are just $u_x = 220\,\text{nm}$ and $u_y = 110\,\text{nm}$, respectively. Thus, the straight nanoplate can be adopted in calculations when we focus on switching the electric and magnetic resonances by polarization. Additionally, Mode #3 and Mode #4 are antisymmetric excitations. Comparing the cases of straight nanoplates, the magnetic fields induced by circular currents are cancelled partly in tapered nanoplates, thereafter, these two excitations becomes much more obvious in tapered nanoplates.

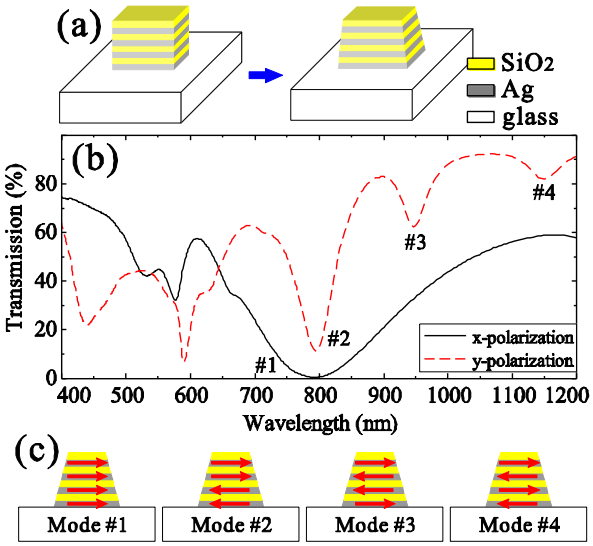

Fig. 5. (a) Configuration of a unit cell with vertical wall as designed, which becomes oblique in fabrication. (b) The calculated normal transmission spectra for the incident polarization (black solid) parallel and (red dashed) perpendicular to the long width, where the side wall of the unit cell is oblique with a tilt angle of about 15°. (c) Schematics of the effective currents induced in multiple Ag layers for the four optical modes marked in (b), respectively.

Furthermore, we try to experimentally demonstrate the electric and magnetic resonances by varying the incident angle. For the incident polarization perpendicular to the short width, the transmission dip at $\lambda \cong 800\,\text{nm}$ shifts to the red as the incident angle θ increases, while the dip at $\lambda \cong 550\,\text{nm}$ disappears, as shown in Figs. 6(a) and (b). For the electric resonance, the electromagnetic field dominates outside the nanoplate, and the interactions between different units are considerable. At the oblique incidence, these interactions will be influenced by phase differences between polarized nanoplates, which lead to the redshift of electric resonance. Contrastively, the magnetic resonance does not shift for the incident polarization perpendicular to the long width, as the transmission dip at $\lambda \cong 800\,\text{nm}$ in Figs. 6(c) and (d). Additionally, this dip becomes shallow when increasing the incident angle θ in the transverse-electric (TE) case, because the in-plane component of incident magnetic field decreases.

#154745 - $15.00 USD Received 16 Sep 2011; revised 16 Oct 2011; accepted 16 Oct 2011; published 27 Oct 2011

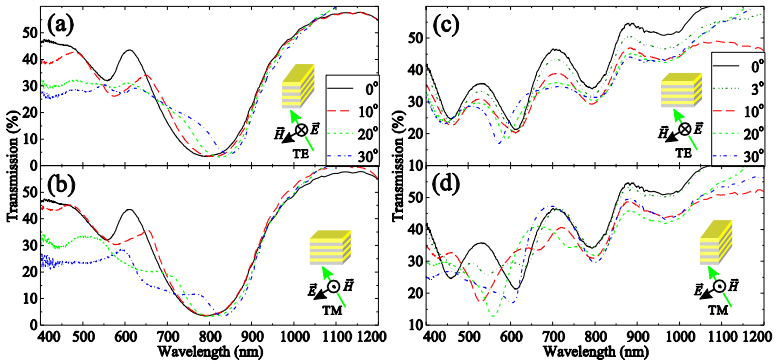

Fig. 6. The measured oblique transmission spectra in the following cases. The polarization is perpendicular to the short width: (a) TE and (b) TM; while the polarization perpendicular to the long width: (c) TE and (d) TM case. The insets schematically illustrate each oblique incidence.

In conclusion, we have demonstrated that in a rectangular multilayered Ag/SiO_2 nanoplate array, the electric and magnetic resonances are switched at the same frequency by changing the polarization of incident light. Actually, two resonances originate from the in-phase and out-of-phase couplings of LSPs on multiple Ag layers respectively, and they are experimentally discriminable in the oblique incidence. The investigations may provide another way to achieve optical magnetism by switching electric resonance to magnetic one, which may be used to construct specific negative-index materials.

Acknowledgments

This work was supported by the State Key Program for Basic Research from the Ministry of Science and Technology of China (Grant Nos. 2012CB921502 and 2010CB630705), the National Natural Science Foundation of China (Grant Nos.11034005, 61077023, and 11021403), and partly by Jiangsu Province (Grant No. BK2008012) and Ministry of Education of China (Grant No. 20100091110029).

#154745 - $15.00 USD Received 16 Sep 2011; revised 16 Oct 2011; accepted 16 Oct 2011; published 27 Oct 2011